Binding of Alkyl Polyglucoside Surfactants to Bacteriorhodopsin and its Relation to Protein Stability

M. Gabriella Santonicola, Abraham M. Lenhoff, and Eric W. Kaler
Center for Molecular and Engineering Thermodynamics, Department of Chemical Engineering, University of Delaware, Newark, Delaware

ABSTRACT The binding of alkyl polyglucoside surfactants to the integral membrane protein bacteriorhodopsin (BR) and the formation of protein-surfactant complexes are investigated by sedimentation equilibrium via analytical ultracentrifugation and by small-angle neutron scattering (SANS). Contrast variation techniques in SANS enable measurement of the composition of the protein-surfactant complexes and determination of the thickness of the surfactant shell bound to the protein. The results indicate that alkyl polyglucosides can bind to BR as single surfactant layers or as a thicker shell. The thickness of the surfactant shell increases with increasing surfactant tail length, and it is generally unrelated to the aggregation number of the micelles even for a small and predominantly hydrophobic membrane protein such as BR. The aggregation numbers determined by sedimentation equilibrium methods match those measured by SANS, which also allows reconstruction of the shape of the protein-detergent complex. When the surfactant is present as a single layer, the BR loses activity, as measured by absorption spectroscopy, more quickly than it does when the surfactant forms a thicker shell.

INTRODUCTION

Study of the interactions between membrane proteins and solubilizing surfactants (or detergents) is an active area of research because of its direct effects on the stability and functionality of these proteins outside of their native biological membranes (1). The ability to preserve protein activity and conformation in solution is also a prerequisite in the choice of optimal surfactants for membrane protein crystallization. Among the various classes of surfactants available or specifically developed for this purpose, the nonionic alkyl polyglucosides are commonly chosen to solubilize biological membranes because of their low toxicity (1,2). Alkyl polyglucosides also aid in the successful crystallization of membrane proteins (3).

Knowledge of how surfactants bind to solubilized membrane proteins can provide a path toward understanding how the surfactant molecules interface with the hydrophobic domains of the protein and affect their structural conformation. Determination of surfactant binding can be accomplished by sedimentation equilibrium analysis in analytical ultracentrifugation experiments. For soluble proteins, such studies are widely used to determine the protein oligomeric states and interactions in solution (4,5), and can be extended to membrane proteins if the effects of bound surfactant are taken into consideration (6). In some cases, the surfactant contribution to the buoyant mass of the complex can be masked by performing experiments in density-matched mixtures of H_2O and D_2O, as proposed by Tanford and Reynolds (7). However, this approach is not feasible in the case of alkyl polyglucosides, because their density is above that of D_2O. The alternative of using solutions with densifiers (such as sucrose or glycerol) is limited by the modifications of surfactant micellization properties and protein activity caused by such additives. For surfactants with a density lower than that of H_2O or higher than that of D_2O, Reynolds and Tanford proposed an approach wherein the molar mass of the protein-detergent complex (PDC) can be calculated by extrapolation of its buoyant mass measured at different solvent densities (8). The amount of bound surfactant can then be estimated if the molar mass of the protein and its oligomeric state are known. This method has been used to determine the association state and the amount of bound surfactant in complexes of the light-harvesting complex LH II and N,N-dimethyldodecylamine N-oxide (LDAO), a surfactant with a density lower than that of H_2O (9). Although the density-matching procedure is limited by accurate determination of the surfactant density, the extrapolation method also suffers from limited applicability. Precise determination of the amount of bound surfactant is possible only in cases where protein samples are highly monodisperse and not prone to aggregation.

Scattering methods are powerful techniques for investigating the structure of colloidal particles and biological macromolecules in solution. In particular, the technique of contrast variation in neutron scattering can selectively highlight parts of assemblies made of different materials that have different scattering-length densities, such as proteins and surfactants. The pair distance distribution function, $p(r)$, obtained from analysis of neutron or x-ray scattering data, reveals the size and shape of aggregates in solution (10). In conformational studies of soluble proteins, this function has been simulated and the computed $p(r)$ compared to measured data to reconstruct a low-resolution structure of the arrangement of protein subdomains (11,12).

Submitted May 19, 2007, and accepted for publication October 24, 2007.

Address reprint requests to Eric W. Kaler, Department of Chemical Engineering, University of Delaware, Newark, DE 19716-3119. Tel.: 302-831-3553; Fax: 302-831-6751; E-mail: kaler@udel.edu.

Editor: Jill Trewhella.

0006-3495/08/05/3647/12 $2.00

doi: 10.1529/biophysj.107.113258

Here we characterize the binding of alkyl polyglucoside surfactants by bacteriorhodopsin using contrast variation studies in both sedimentation equilibrium and small-angle neutron scattering experiments. Bacteriorhodopsin (BR) is an integral membrane protein found in the purple membrane of *Halobacterium salinarum*. One of the first membrane proteins to be crystallized, BR is the most extensively studied transmembrane protein and its structure and molecular mechanism are known at atomic resolution (13,14). BR is a retinal-bound protein that pumps protons across the cellular membrane when it is exposed to light. Most of the mass of BR (~80%) is embedded in the bilayer region, with ~30 lipid molecules per protein trimer (15). The active form of BR in purple membrane exhibits a characteristic absorption maximum around 568 nm. This absorption peak shifts to 550 nm for monomeric BR after solubilization in surfactant solutions. Both the trimers and the individual monomers of BR are active in pumping protons (16).

The alkyl-β-monoglucosides $C_8\beta G_1$ and $C_9\beta G_1$ and the alkyl-β-maltosides $C_8\beta G_2$, $C_9\beta G_2$, $C_{10}\beta G_2$, and $C_{12}\beta G_2$ were chosen for study because BR could be solubilized into a single homogeneous phase with these surfactants at room temperature. The effect of systematically changing the alkyl chain length of the glucoside while keeping the headgroup properties constant was investigated. Furthermore, the protein-surfactant assembly was modeled using an atomistic approximation wherein the form factor and pair distance distribution function of the aggregate can be computed. Comparing these functions with experimental data provides insight into the distribution of surfactant around the protein. Finally, the properties of surfactant binding to BR are related to the stability of the membrane protein as determined by absorption spectroscopy.

EXPERIMENTAL METHODS

Materials

Alkyl-β-monoglucosides ($C_8\beta G_1$ and $C_9\beta G_1$) and alkyl-β-maltosides ($C_8\beta G_2$, $C_9\beta G_2$, $C_{10}\beta G_2$, and $C_{12}\beta G_2$) of the highest purity (Anagrade, >99%) were purchased from Anatrace (Maumee, OH) and used as received. Deuterium oxide (DLM-4, 99.9% deuterated) was obtained from Cambridge Isotope Laboratories (Andover, MA). Buffer salts were purchased from Sigma-Aldrich (St. Louis, MO) and were of the purest grade.

Surfactant preparation and characterization

Surfactant solutions were prepared by dissolving a weighed amount of the alkyl polyglucoside in aqueous or deuterated solvents buffered at pH 5.5 with 25 mM potassium phosphate. The acidity of buffer solutions in D_2O was corrected to take into account the difference in pH meter reading between H_2O and D_2O solutions ($pD = pH_{reading} + 0.4$) (17). Solution densities were measured using an Anton Paar DMA 60 density meter with measuring cell DMA 602 (Anton Paar, Graz, Austria). The temperature of the measuring cell was controlled with a circulating water bath stable to ± 0.01°C.

The critical micelle concentrations of the surfactants were determined by isothermal titration calorimetry using a VP-ITC microcalorimeter (MicroCal, Northampton, MA). Experiments were conducted at 20°C. In each experiment, 40 aliquots (6 μL each) of a concentrated solution of the alkyl polyglucoside were automatically injected into the sample cell initially filled with pure buffer. The critical micelle concentration (CMC) value was determined at the point where the first derivative curve of the enthalpogram displays an extremum (18).

Protein sample preparation

Bacteriorhodopsin was extracted from the purple membrane of *H. salinarum* (strain ET1001) as described by Dencher and Heyn (19). The solubilized BR was of optical purity, A_{280}/A_{550}, ~1.6. BR concentrations were determined spectroscopically at room temperature using molar extinction coefficients of 62,700 M^{-1} cm^{-1} at 568 nm, measured for light-adapted BR in purple membrane (20), and 58,000 M^{-1} cm^{-1} at 550 nm for solubilized BR (19). The molecular mass of the retinal-bound protein (27,092 g mol^{-1}) was calculated from its amino acid sequence and used in all calculations relative to the active form of monomeric BR.

Samples containing BR were prepared using freshly extracted protein (within 24 h). The removal and subsequent exchange of surfactant were carried out by diafiltration on Amicon Ultra-4 filters (Millipore, Billerica, MA) with 30,000 MW cut-off using 25 mM phosphate buffer at pH 5.5 containing 30 mM of $C_8\beta G_1$ (CMC ~25 mM). A 20-step diafiltration with equivalent volumes of this exchange buffer could be performed in a few hours and caused no detectable loss of protein activity, yielding a final sample of excellent optical purity ($A_{280}/A_{550} = 1.55$ and $A_{385}/A_{550} = 0.20$). A phospholipid assay (21) showed that the overall delipidation of the protein-surfactant complex was ~70%. Complete delipidation was avoided as BR has very limited stability in that state (22). The final concentration of alkyl glucoside in the protein samples was verified using the anthrone method, a colorimetric assay developed for the quantification of carbohydrates and adapted to solutions of surfactants with glucose headgroups (23).

Protein/surfactant solutions with different levels of deuteration were prepared by mixing appropriate volumes of stock solutions made in aqueous and fully deuterated buffers. These two stocks were prepared by extensively washing the protein solutions with the desired buffer in centrifugal filters (Amicon Ultra-4, Millipore). Surfactant concentrations were chosen to be ~10 mM above the CMC so that the number of molecules available to bind to the protein in the micellar phase was comparable for all the surfactants.

In protein stability studies, UV-visible spectra of BR were collected using a Lambda 2 spectrophotometer (Perkin-Elmer, Wellesley, MA). Small aliquots of protein samples were spun before each measurement and the supernatant absorbance was measured using quartz microcuvettes.

Analytical ultracentrifugation

Sedimentation equilibrium experiments were performed in an Optima XL-I analytical ultracentrifuge from Beckman Coulter (Fullerton, CA) using photoelectric absorption optics for the protein solutions and Rayleigh interference optics for the surfactant solutions. The centrifuge was equipped with a four-place An-60 Ti analytical rotor. Samples were loaded in six-sector cells with Epon charcoal-filled centerpieces (optical path length, 12 mm) assembled between two windows made of optical-grade quartz for absorbance or sapphire for interference. All experiments were conducted at 20°C. Achievement of equilibrium conditions was established by comparing scans recorded every 2 h until the distribution profiles were invariant with time.

In experiments with absorption optics, sample volumes were 110 μL for protein solutions and 125 μL for the reference solvent. A radial step size of 0.001 cm and 10 averages per scan were used. Protein concentration distributions were recorded at 550 nm, which corresponds to the absorption of retinal-bound monomeric BR in its active state. Protein samples with initial concentrations in the range 0.3–0.5 OD/cm at 550 nm were measured, corresponding to concentrations of active BR of 6–10 μM. In experiments with interference optics, sample volumes were 110 μL for surfactant solutions and

115 μL for the reference solvent (buffer). The detection wavelength was 675 nm. A blank correction for window distortion on the fringe displacement data was performed at the same equilibrium speed using water in both the solution and the reference channel (24).

Sedimentation equilibrium data were evaluated by fitting the absorption profiles as a function of radial distance in the cell at equilibrium. For a single noninteracting species in solution, the equilibrium distribution is described by (25,26)

$$c(r) = c(r_0) \times e^{\left[M_c(1-\overline{\nu}_c\rho)\frac{\omega^2}{2RT}(r^2-r_0^2)\right]}, \quad (1)$$

where M_c and $\overline{\nu}_c$ are the molar mass and partial specific volume of the protein-surfactant complex, respectively, ρ is the solvent density, and ω is the rotor speed. M_c and $\overline{\nu}_c$ were obtained independently from the buoyant molar mass of the complex $M_b = M_c(1 - \overline{\nu}_c\rho)$ measured at different solvent densities (26). M_c and $\overline{\nu}_c$ were then related to the composition of the complex by

$$M_c = M_p(1 + \sum_i \delta_i) \quad (2)$$

and

$$\overline{\nu}_c = \frac{(\overline{\nu}_p + \sum_i \overline{\nu}_i)}{(1 + \sum_i \delta_i)}, \quad (3)$$

where δ_i is the amount (g/g protein) of bound component (surfactant and lipid) in the complex, and the subscript p refers to the protein component of the complex. For BR, M_p was calculated from the sequence as described above. Eq. 2 was then used to evaluate δ_{surf} once the oligomeric state of the protein in the complex at the solution condition was known.

In the case of alkyl polyglucoside surfactants, with densities larger than that of D_2O, M_c and $\overline{\nu}_c$ were determined by extrapolating the fitted line of the experimental buoyant molar masses beyond the measured range of solvent densities. The buoyant molar masses obtained at different levels of solvent deuteration were first corrected for deuterium substitution of the complex labile hydrogens. In a fully or partially deuterated solvent, isotopic substitution increases and decreases M_c and $\overline{\nu}_c$, respectively, giving an apparent buoyant mass (27)

$$M_b = M_c(k - \overline{\nu}_c\rho), \quad (4)$$

where k is the ratio of the deuterated molar mass of the complex to the nondeuterated mass and can be expressed as

$$k = \frac{M_c + H_{ex}f}{M_c}, \quad (5)$$

where H_{ex} is the number of exchangeable hydrogens in the complex and f is the fraction of deuteration of the solvent.

After extraction and surfactant exchange, BR solutions contained approximately three lipids per protein monomer, as determined by phosphorus analysis. Assuming that the lipid composition of purple membrane was that reported by Renner et al. (28), the mass of lipid in the complex was estimated to be 2700 g/mol/BR monomer. The lipid contribution to the buoyant mass of the complexes was estimated after separating the contribution of each component using (8)

$$M_c(1 - \overline{\nu}_c\rho) = M_p\big[(1 - \overline{\nu}_p\rho) + \delta_{surf}(1 - \overline{\nu}_{surf}\rho) + \delta_{lip}(1 - \overline{\nu}_{lip}\rho)\big]. \quad (6)$$

The partial specific volume of BR (0.747 cm^3/g) was calculated from the amino acid sequence using the mean residue volumes (29) and it was corrected for temperature (30). The lipid contribution to the complex from Eq. 6 was estimated to be 0.5% by weight at most, and was therefore neglected in the analysis of sedimentation equilibrium data.

The analysis of sedimentation equilibrium data with Eq. 1 was performed by nonlinear least squares (Levenberg-Marquardt algorithm) and the global fitting package provided in Igor Pro software (WaveMetrics, Lake Oswego, OR). At each solution condition, the buoyant molar mass M_b was globally fitted among equilibrium profiles recorded at two or three rotor speeds, chosen to be significantly different (31). For most of the surfactants, experiments were run at speeds in the range 9000–20,000 rpm, except for $C_9\beta G_1$ and $C_{12}\beta G_2$, where speeds from 7000 to 12,000 rpm were used.

BR was found to be stable in the monoglucosides $C_8\beta G_1$ and $C_9\beta G_1$ for a few days at 20°C, and analytical ultracentrifugation experiments could be run at three different velocities consecutively for 2 days. On the other hand, due to the limited stability of BR in the short-chain maltosides at 20°C, experiments were run at each velocity using a fresh sample.

Small-angle neutron scattering

In the small-angle neutron scattering (SANS) experiments, performed at the Center for High Resolution Neutron Scattering of the National Institute of Standards and Technology (NIST) in Gaithersburg, MD, the scattered neutron intensities were measured as a function of the magnitude of the scattering vector, $q = 4\pi/\lambda \sin(\theta/2)$, where θ is the angle between the scattered and incident beams. Here, the average neutron wavelength was 6 Å, with a spread $\Delta\lambda/\lambda$ of 15%. Data were collected on the NG-3 instrument at sample-detector distances of 1.33 m, 4.5 m, and 13.2 m (with a detector offset of 25 cm from the center at the shorter distances and 10 cm at 13.2 m), covering a q-range of 0.004 to 0.5 $Å^{-1}$. The target protein concentration in all samples was 1 mg/mL. All experiments were carried out at 20°C and within 24 h after sample preparation. Because of the sensitivity to light of retinal-bound bacteriorhodopsin, measurements were conducted in the dark by covering the sample chamber windows. The raw scattering data were corrected for solvent, empty cell, and buffer solution scattering, all measured separately, and placed on an absolute scale using standards calibrated by NIST. The incoherent background was calculated from a Porod plot for values of $q > 0.25$ $Å^{-1}$ and subtracted from the scattering data before analysis.

Contrast variation experiments were performed in solvents with deuteration levels of 0, 25, 50, 75, and 100%. Solutions with D_2O content <50% were held in quartz cells with 1 mm optical path length, whereas 2-mm cuvettes were used for samples with D_2O content of 50% and above. Scattering from the corresponding hydrogenated and partially deuterated buffer solutions was measured separately and subtracted from the protein/surfactant intensities before Guinier analysis.

The scattering-length densities of surfactants and proteins were calculated from the tabulated atomic coherent scattering lengths (32) and the atomic volumes. Surfactant volumes were calculated from partial specific volumes obtained by density measurements with an accuracy of 1.0%. The molecular volume of BR was obtained from the partial specific volume calculated from the amino acid sequence (29). The calculation of the scattering length density for both proteins and surfactants takes into account the extent of hydrogen/deuterium substitution that occurs when the molecule is dissolved in a deuterated buffer. For the alkyl monoglucoside surfactants, the four labile hydrogens on the headgroup were assumed to be fully exchangeable. For proteins, hydrogens bound to nitrogen and oxygen (on peptide bonds and side chains of amino acid residues) readily exchange when they are exposed to deuterated solvent. The exchange can be considered complete for hydrogens on residues on the exterior of the protein, whereas peptide protons that are buried in the protein core or involved in secondary structure hydrogen bonding exchange slowly (33). The extent of the hydrogen exchange on the protein peptide backbone depends on sample preparation procedures and experimental conditions. Previous work on BR in purple membrane has shown that ~20% of peptide hydrogens exchange in the first 2 h of exposure to D_2O, followed by a gradual exchange that reaches values of 45% for dark-adapted samples and 38% for illuminated samples over a 40-h period (34,35). In this work, 40% of the hydrogens on BR peptide backbone were considered exchanged with deuterium, in addition to residue side chains. This

corresponds to 215 exchanged protons, and to an average $\overline{\rho}$ for BR of 2.36×10^{-6} Å^{-2}.

SANS data analysis

Analysis of the scattering data was carried out either by directly fitting the scattering profiles using shape-dependent models (36), or by applying the method of indirect Fourier transformation (IFT) (37,38). When fitting the SANS data using shape-dependent models, a least-squares procedure was implemented, and the goodness of the fit was assessed through the chi-squared (χ^2) parameter (36).

The IFT method allows simultaneous determination of the form factor and structure factor without assuming a model for the shape of the particles. Under the decoupling approximation (39), the total scattered intensity $I(q)$ can be written as the product of the form factor P(q), which represents the contribution to the scattered intensities from the particle geometry, and the structure factor S(q), with contributions from interparticle interactions,

$$I(q) = n_{\mathrm{p}} P(q) S(q), \tag{7}$$

where n_{p} is the number density of particles in solution. In dilute solutions, interparticle interactions are negligible ($S(q) \approx 1$) and the scattering intensity is related to the pair distance distribution function, $p(r)$, by the Fourier transformation

$$I(q) = 4\pi \int_0^{\infty} p(r) \frac{\sin(qr)}{qr} dr. \tag{8}$$

Modeling of PDCs by the sphere method

The sphere method is a technique that enables the simulation of the scattering function and the distance distribution function p(r) of objects with arbitrary shape for small-angle scattering experiments (40). The scattering object (the PDC) was built by assembling two subunits: the protein core and the surfactant shell. The atomic coordinates in the protein subunit were taken from file 1QHJ (13) in the Protein Data Bank, a 1.9 Å resolution data set that includes the retinal moiety. The surfactant component was modeled as a hollow cylinder surrounding the hydrophobic region of the protein. Each subunit was made of spheres of radius 1 Å to fill up the required volume, and it was weighted by the difference of scattering length densities (or contrast) between the subunit and the solvent. No effects due to interparticle interference were included in this calculation.

RESULTS

Activity of solubilized BR by UV-visible spectroscopy

The activity of retinal-bound BR in the various surfactant solutions was monitored over time via the absorption ratio A_{280}/A_{550}. Samples with high optical purity (~1.6) were obtained immediately after extraction and removal of excess $C_8\beta G_1$ using a phosphate buffer at pH 5.5. After surfactant exchange, BR showed approximately the same optical purity (~1.7) in all the alkyl polyglucosides studied. BR samples were then kept at 4°C and in the dark for 14 days. Absorption spectra were measured at intervals of 2 days and used to plot the ratio A_{280}/A_{550} versus time in solutions of alkyl-β-monoglucosides and alkyl-β-maltosides (Fig. 1). For each set of alkyl polyglucoside homologs, the surfactant's ability to preserve BR activity correlates directly with the length of the alkyl tail, so longer-chain maltosides (C_{10} and C_{12}) and

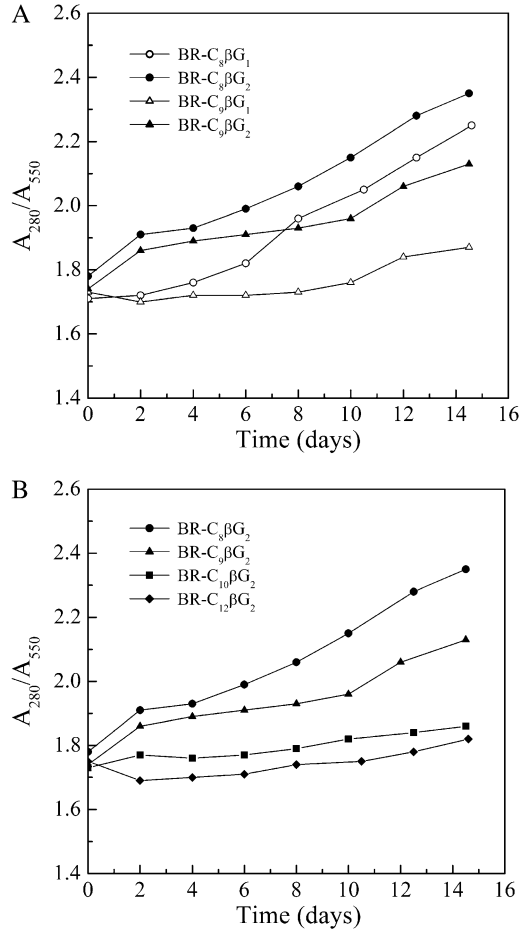

FIGURE 1 Comparison of bacteriorhodopsin stability in solutions of alkyl polyglucosides with C_8 and C_9 tails (*A*) and in solutions of alkyl-β-maltosides with tails C_8–C_{12} (*B*).

$C_9\beta G_1$ are the best choice to maintain BR activity for more than a few days.

Sedimentation equilibrium of micellar aggregates

For each surfactant, the effective molar mass, and consequently the micellar aggregation number (Table 1), was calculated from the micellar buoyant mass measured by analytical ultracentrifugation and the solvent density and the partial specific volume of the surfactant found by densimetry (41). The aggregation numbers of $C_8\beta G_1$, $C_8\beta G_2$, and $C_{12}\beta G_2$ are in good agreement with values reported in the literature (1,44). For $C_9\beta G_2$ and $C_{10}\beta G_2$, lower values of the aggregation numbers were reported by the manufacturer (Anatrace). However, these values were obtained by static light scattering, and they are valid at surfactant concentrations very close to the CMC (so that the concentration of micellar aggregates is nearly zero) due to the use of extrapolation. Values measured by sedimentation equilibrium are unaffected by this limitation and represent actual micellar

TABLE 1 Properties of complexes of bacteriorhodopsin and $C_i\beta G_j$ as determined by sedimentation equilibrium experiments at 20°C in 25 mM potassium phosphate buffer

BR-surfactant complex	M_c (Da)	$\bar{v}_c$ (cm^3/g)	Bound surfactant (mol/mol protein)	Micelle N_{aggr}
BR-$C_8\beta G_1$	60,800 ± 2100	0.820 ± 0.041	115 ± 7	93
BR-$C_9\beta G_1$	85,900 ± 3100	0.836 ± 0.043	192 ± 10	637
BR-$C_8\beta G_2$	83,700 ± 2900	0.789 ± 0.041	125 ± 6	47
BR-$C_9\beta G_2$	91,000 ± 3300	0.798 ± 0.055	136 ± 7	63
BR-$C_{10}\beta G_2$	103,500 ± 4100	0.814 ± 0.046	158 ± 8	80
BR-$C_{12}\beta G_2$	118,400 ± 4000	0.823 ± 0.040	179 ± 8	135

The number of bound surfactant monomers is calculated considering 40% hydrogen/deuterium exchange of BR labile peptide hydrogens and full exchange of the surfactant shell. Micellar aggregation numbers refer to measurements by sedimentation equilibrium of surfactant solutions with concentration CMC + 10 mM.

masses even when micellar growth occurs above the CMC. In the case of $C_8\beta G_1$, measurements were also obtained at 70 mM surfactant concentration. The micellar aggregation number was found to be 127, which is 37% larger than that for micelles in solution at 35 mM $C_8\beta G_1$. Control samples with surfactant concentrations below the CMC were run to assess the influence of the free surfactant on the measurements, and showed no fringe displacement at the rotor speeds used to evaluate the micellar buoyant masses.

Sedimentation equilibrium of bacteriorhodopsin-surfactant complexes

The structures of BR complexes in solutions of various alkyl monoglucosides and alkyl maltosides were examined. For each surfactant a series of 0, 25, 50, 75, and 100% buffer deuteration was used. The apparent buoyant molar mass obtained from the global fitting of the concentration profiles was corrected for isotopic substitution of the protein labile hydrogens, as well as the exchangeable hydrogens of the bound glucoside molecules (see Methods). A peptide hydrogen exchange of 40% was assumed, with 215 total exchanged hydrogens per BR molecule ($k = 1.008$). This value is also very close to the number calculated by considering exchange of the protein hydrophilic residues only (218 hydrogens). For BR solubilized in surfactant solutions the extent of hydrogen peptide exchange may differ from that in purple membrane due to an increase of water accessibility in the interior regions of the delipidated protein. However, the difference between complete and partial peptide hydrogen substitution (142 hydrogens) would change the molecular mass of BR by only ~0.5%, and this change would have a negligible effect on the calculated amount of bound surfactant.

For alkyl polyglucoside surfactants, the number of labile hydrogens on the headgroup (4 H^+/molecule for monoglucosides and 7 H^+/molecule for maltosides, all of which are completely exchangeable) contributes significantly to the increase of the complex mass in deuterated and partially deuterated solutions, and cannot be neglected. However, the amount of bound surfactant is not known a priori. To take into account this contribution, an iterative procedure was used wherein the value of k was adjusted to include the total number of hydrogens exchanged by the surfactant component of the complex.

The monomeric state of BR in all the surfactants used was confirmed based on the absorption maximum at ~550 nm of monomeric, active BR in its light-adapted form solubilized in $C_8\beta G_1$. After each surfactant exchange, no shift in the absorption peak could be observed, suggesting that the retinal-bound protein retains its monomeric form when bound to the other alkyl polyglucosides at the concentrations used here.

The monodispersity of the sedimenting species was assessed by plotting $\ln(c)$, or equivalently $\ln(A)$, versus r^2, according to Eq. 1. The linearity of the plots indicated that the solutions contain monodisperse protein-surfactant complexes, so the single-species model used in fitting the concentration profiles is a valid approximation. For each surfactant, radial absorption profiles at three different rotor speeds were globally fitted to obtain the buoyant mass of the complex. Results of this analysis for BR-$C_9\beta G_1$ complexes are reported in Fig. 2.

To determine the mass of alkyl polyglucoside bound to BR, density contrast variation studies were carried out using mixtures of hydrogenated and deuterated buffers. Fig. 3 shows the buoyant molecular mass of complexes of BR with alkyl monoglucosides and alkyl maltosides as a function of

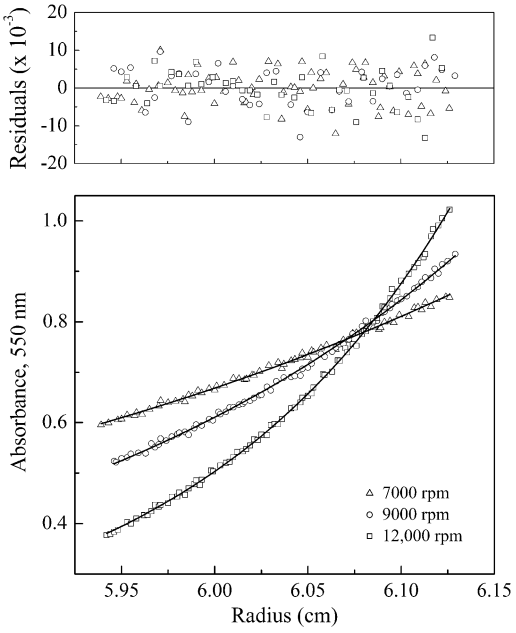

FIGURE 2 Results of the global fitting of radial absorbance profiles collected at three different velocities for BR-$C_9\beta G_1$ complexes in aqueous buffer (25 mM potassium phosphate, pH 5.5) at 20°C. Concentrations of active BR and $C_9\beta G_1$ are 8 μM and 15 mM, respectively. The residuals of the fit are shown above the absorbance profiles.

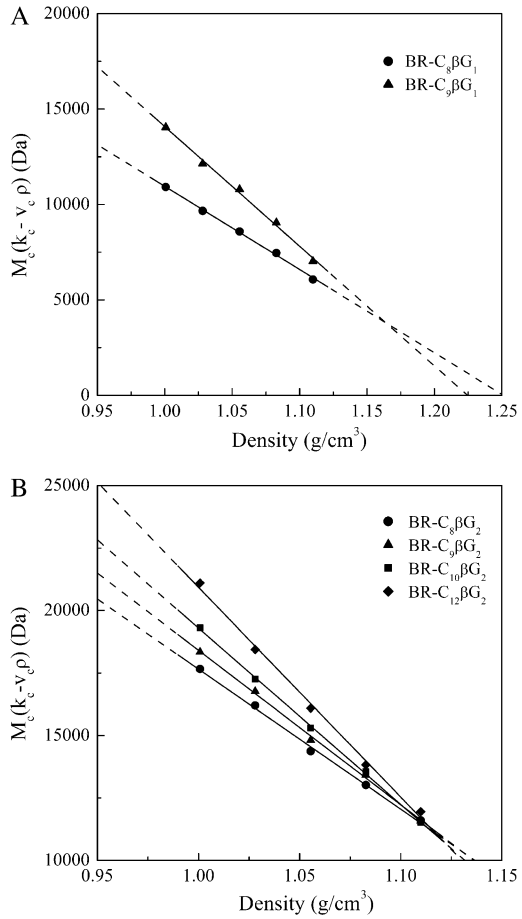

FIGURE 3 Buoyant molar mass of bacteriorhodopsin-surfactant complexes as a function of solvent density in solutions of alkyl-β-monoglucosides (*A*) and of alkyl-β-maltosides (*B*) at 20°C. Error bars on the individual data points are smaller than the symbols.

the solvent density. The molar masses and partial specific volumes of the complexes of BR and individual surfactants were evaluated using the extrapolation procedure described above (Table 1). Except for solutions of $C_8\beta G_1$ and $C_{12}\beta G_2$, the number of surfactant molecules bound by BR is mostly unrelated to the micellar aggregation numbers. In solutions of maltosides with alkyl chains C_8 to C_{10}, BR binds large amounts of the amphiphile, and the amount bound is not comparable to the aggregation number of the individual micelles. In contrast, when $C_9\beta G_1$ is used to solubilize BR, each protein monomer is surrounded by an amount of surfactant that is approximately one-third of that needed to form a $C_9\beta G_1$ micelle.

Experiments on BR samples with 20 mM $C_8\beta G_1$ were also performed, although this concentration is below the surfactant CMC (25 mM). The nonrandomness of the residual plots from the global fitting procedure and the curvature observed in the graphs of ln(*A*) versus r^2 indicate that BR was highly aggregated, confirming that optimal solubilization of membrane proteins occurs only at surfactant concentrations above the CMC.

Surfactant shell geometry from sedimentation equilibrium data

A structural interpretation of the above results was obtained by modeling the surfactant bound to BR as a shell surrounding the hydrophobic transmembrane domain of the protein. The shell length was set equal to the hydrophobic thickness of BR (30 Å) (45). The shell thickness for each surfactant was then calculated from the volume of the amphiphile bound by BR determined in the sedimentation equilibrium and densimetry experiments.

The size of the BR core in the complex and, consequently, the inner dimension of the surfactant shell were estimated from the crystal structure. The hydrophobic domain of BR was then represented as a cylinder of elliptic section with major and minor axes of 30 Å and 20 Å, respectively. Table 2 compares the resulting calculated thickness of the BR surfactant shell in various solutions of alkyl polyglucosides and the calculated amphiphile length. The tail length of the surfactant was calculated using the Tanford expression and was multiplied by 0.8 to account for the fact that hydrocarbon chains in the micellar interior are not fully extended (46). The length of one glucose headgroup was estimated to be 4 Å from its molecular structure and dimensions.

SANS contrast variation studies of BR-surfactant complexes

Contrast variation studies in SANS are useful for determining the composition of protein-surfactant complexes. At the point where the scattering-length density of the complex matches that of the solvent, contributions of the protein and surfactant parts to the coherent scattering length of the complex can be separated using

$$V_p(\overline{\rho}_p - \overline{\rho}_{solv}) = V_{surf}(\overline{\rho}_{surf} - \overline{\rho}_{solv}), \quad (9)$$

where $\overline{\rho}_p$, $\overline{\rho}_{surf}$, and $\overline{\rho}_{solv}$ are the average scattering length densities of protein, surfactant, and solvent, respectively, evaluated at the complex match point. The surfactant mass in the complex (M_{surf}) can then be calculated from

$$\frac{M_{surf}}{M_p} = \frac{(\overline{\rho}_p - \overline{\rho}_{solv})\overline{\nu}_p}{(\overline{\rho}_{surf} - \overline{\rho}_{solv})\overline{\nu}_{surf}}, \quad (10)$$

TABLE 2 Comparison of the surfactant shell thickness bound to bacteriorhodopsin from sedimentation equilibrium data and the surfactant length

BR-surfactant complex	Shell thickness (Å)	Surfactant length (Å)
BR-$C_8\beta G_1$	13.3 ± 0.6	13.3
BR-$C_9\beta G_1$	20.2 ± 0.7	14.3
BR-$C_8\beta G_2$	18.0 ± 0.6	17.3
BR-$C_9\beta G_2$	19.7 ± 0.7	18.3
BR-$C_{10}\beta G_2$	22.4 ± 0.8	19.4
BR-$C_{12}\beta G_2$	25.8 ± 0.8	21.4

Surfactant length was calculated according to Tanford (46).

where $\overline{\nu}_p$ and $\overline{\nu}_{surf}$ are the partial specific volumes of protein and surfactant, respectively.

The contrast match point of the protein-surfactant complexes was obtained from SANS experiments in solvents with different levels of deuteration. In dilute solutions, where interparticle interference is negligible, the intensity scattered from the complexes is

$$I(q) = n_c(\overline{\rho}_c - \overline{\rho}_{solv})^2 V_c^2 P(q), \quad (11)$$

where the subscript c refers to the complex. For $q \to 0$, the form factor of the complex $P(q)$ is unity, and the scattered intensity is proportional to the square of the contrast,

$$I(0) = n_c(\overline{\rho}_c - \overline{\rho}_{solv})^2 V_c^2. \quad (12)$$

The scattering-length density of the complex can then be determined at the point where the intensity scattered from the solution becomes negligible.

The scattering profiles of protein-surfactant complexes in solvents with different levels of deuteration were fitted using the Guinier equation (47),

$$I(q) = I(0)\exp\left(\frac{-R_g^2 q^2}{3}\right), \quad (13)$$

which is valid in the q-region where $qR_g \leq 1$. Here R_g is the radius of gyration of the protein-surfactant complex and $I(0)$ the extrapolated intensity at $q = 0$. Fig. 4 shows the Guinier analysis for SANS data from BR solubilized in solutions of $C_9\beta G_1$ (15 mM). Data uncertainty increases with the H_2O content of the solvent due to the larger incoherent scattering from the background aqueous buffers.

Applying Eq. 12, the fitted values of $I(0)$ were normalized by the protein and surfactant concentrations, and the square-root values were plotted as a function of the percentage of D_2O in the solvent. This V-shaped plot displays a minimum near the contrast match point. The negative root of $\sqrt{I(0)/c}$ was taken for samples with D_2O concentration past the minimum, and the contrast match point of the complex was determined from the intersection of the fitted line through these square-root values with the x axis. Fig. 5, *A* and *B*, shows such an analysis for BR-$C_8\beta G_1$ and BR-$C_9\beta G_1$ complexes, respectively.

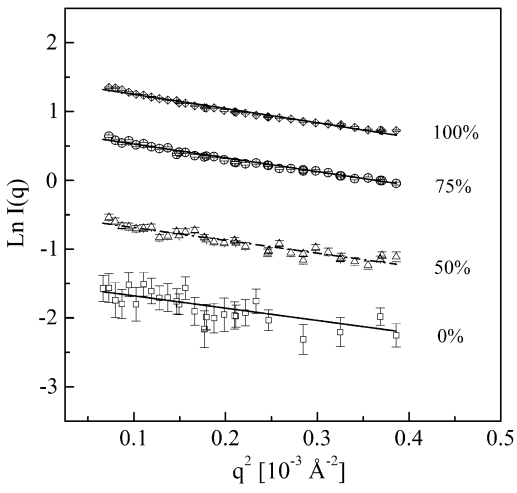

FIGURE 4 Guinier profiles of BR-$C_9\beta G_1$ complexes in buffers with various D_2O contents (25 mM potassium phosphate, pH 5.5). Protein and surfactant concentrations were 1 mg/mL and 15 mM, respectively.

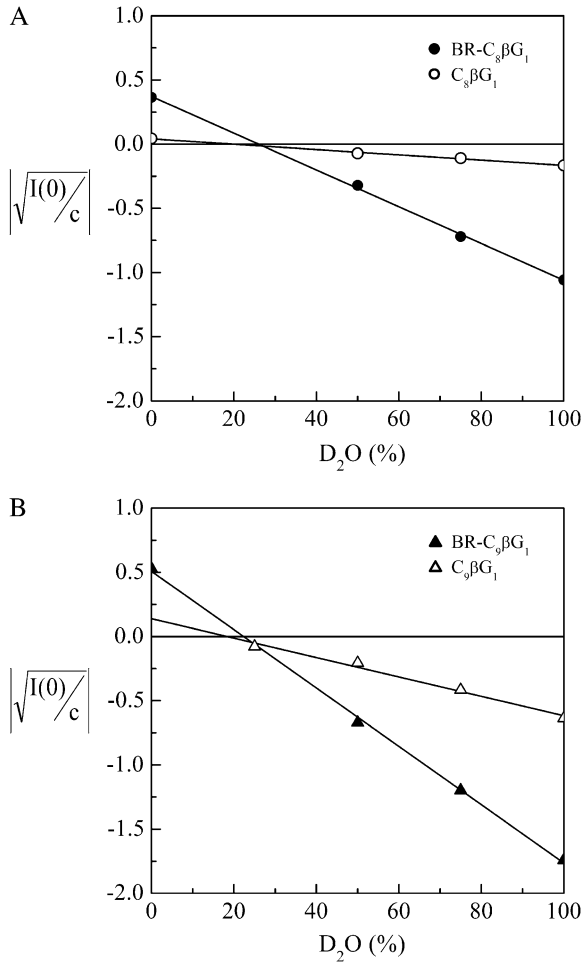

FIGURE 5 The positive or negative value of the square root of zero-angle scattering from BR-$C_8\beta G_1$ complexes (*A*) and BR-$C_9\beta G_1$ complexes (*B*), and the corresponding protein-free micellar solutions. Data points are normalized by protein and surfactant concentrations (mg/mL). Error bars on single data points are smaller than the symbols.

The contrast match points for the protein-surfactant complexes and the micelles are summarized in Table 3. Contrast variation experiments were also performed on BR solubilized in a mixture of deuterated and hydrogenated $C_8\beta G_1$ (70:30 mol ratio). Note that the amount of surfactant bound by BR in solutions of $C_8\beta G_1$ (~121 molecules) is comparable to that bound in the mixture d-$C_8\beta G_1$/$C_8\beta G_1$ (~106 molecules), showing that there is no effect of surfactant deuteration on the composition of the protein-surfactant complexes.

TABLE 3 Contrast match points of bacteriorhodopsin-surfactant complexes and their corresponding protein-free micelles

Protein-surfactant complexes	Match point (D_2O %)	Bound surfactant (mol/mol protein)
BR-$C_8\beta G_1$	25.9 ± 1.5	121 ± 35
BR-$C_9\beta G_1$	23.1 ± 0.9	235 ± 46
BR-(d-$C_8\beta G_1$/$C_8\beta G_1$) (70/30 mol)	63.6 ± 2.9	106 ± 23
	Match point (D_2O %)	
Micelles	Experimental	Theoretical
$C_8\beta G_1$ (35 mM)	19.8 ± 3.7	18.7
$C_9\beta G_1$ (15 mM)	18.3 ± 5.8	17.7
d-$C_8\beta G_1$/$C_8\beta G_1$ 70/30 mol (35 mM)	81.0 ± 6.0	81.5

Contrast match points were determined by small-angle neutron scattering in potassium phosphate buffer (25 mM, pH 5.5) at 20°C. Protein concentration is ~1.0 mg/mL. Values of the bound surfactant are calculated assuming 40% exchange of bacteriorhodopsin peptide hydrogens.

Analysis of the full spectra for membrane protein-surfactant solutions

The SANS data from the protein-surfactant solutions in fully deuterated solvent were analyzed for insight into the size and shape of the PDCs, and how these compare with the features of the micelles in the protein-free solutions. Fig. 6 shows data from solutions with BR and $C_8\beta G_1$ (35 mM), and BR and $C_9\beta G_1$ (15 mM). In both cases, the scattering profiles are compared with those from the corresponding micellar solutions. Data from micellar solutions were fitted directly using shape-dependent models. The micelles of $C_8\beta G_1$ were best fitted with cylinders having a radius equal to the length of the surfactant molecule (13.3 Å), and a length of 67 Å. The lengths of the surfactant molecules were calculated by adding the contributions from headgroups and alkyl chains, as described above. Micelles of $C_9\beta G_1$ can be best fitted with a model for semiflexible cylinders (48), where radius, Kuhn length, and contour length are 14.4 Å, 236 Å, and 435 Å, respectively. The scattering models used in both cases consider excluded volume effects, but neglect other intermicellar interactions because the surfactant solutions are dilute (10 mM in excess of the CMC).

The micellar dimensions determined from SANS can be used to calculate the volume of the micelles, and hence their aggregation numbers. For these calculations, the individual surfactant volumes were obtained from density measurements at the same conditions as in the SANS experiments. The estimated aggregation numbers of the micelles formed in solutions of 35 mM $C_8\beta G_1$ and of 15 mM $C_9\beta G_1$ are 89 and 632, respectively.

The SANS profiles from the PDC solutions were analyzed using the IFT technique, which allows determination of the particle form factor and pair distance distribution function without assuming a model for its shape. Fig. 7 *A* shows the calculated pair distance distribution functions for both the BR-$C_8\beta G_1$ complexes and the $C_8\beta G_1$ micelles. Micelles in

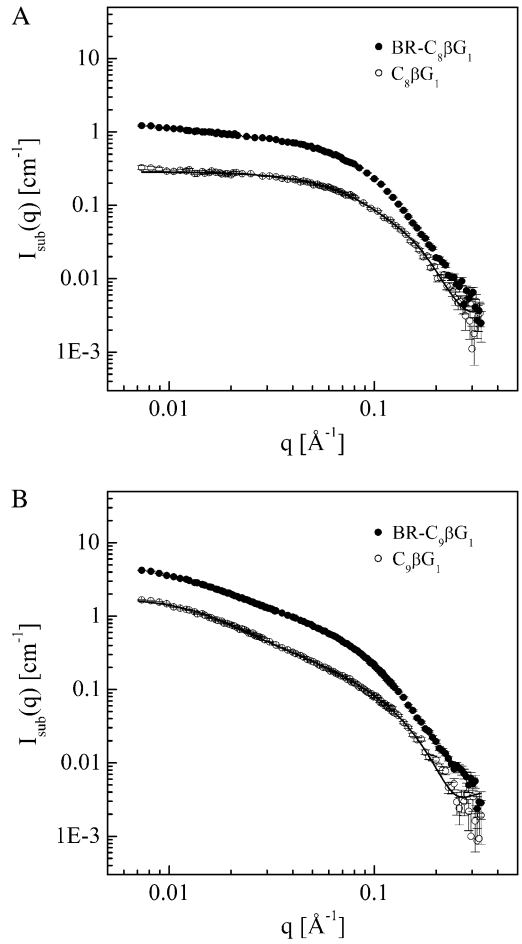

FIGURE 6 SANS data for BR-$C_8\beta G_1$ (*A*) and BR-$C_9\beta G_1$ (*B*) complexes and their corresponding micellar solutions (*open symbols*) in fully deuterated buffer (25 mM potassium phosphate, pD 5.5) at 20°C. Protein concentration was 1 mg/mL. Concentrations of $C_8\beta G_1$ and $C_9\beta G_1$ were 35 mM and 15 mM, respectively. The solid lines are the best fit to the micelles in protein-free solutions.

solutions of 35 mM $C_8\beta G_1$ have an elongated shape with a maximum length of ~70 Å, in agreement with the results obtained above by directly fitting the scattering data to the cylindrical micelle model. On the other hand, the PDCs are more globular than the micelles and the thickness of the object, which is denoted by the position of the peak of the function $p(r)$, is larger than that of the corresponding micelles.

For BR solubilized in $C_9\beta G_1$ solutions, the interpretation of the IFT analysis becomes more challenging. The pair distance distribution function of the micelles shows a significant shoulder after the first peak (Fig. 7 *B*). Generally, shoulders similar to this indicate the presence of intermicellar interactions. Since the investigated surfactant solution is dilute (micelle volume fraction $= 2 \times 10^{-3}$), these interactions are likely to be of an intramicellar nature reflecting the interactions of the locally rigid cylinders that form the semiflexible micelle. After BR is solubilized in the $C_9\beta G_1$ solution, the shoulder decreases significantly. This suggests,

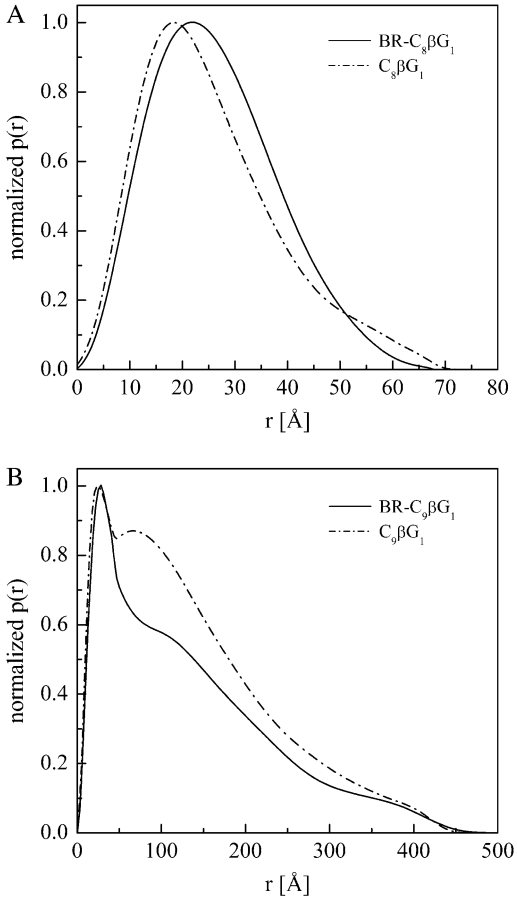

FIGURE 7 Pair distance distribution functions from IFT analysis for BR-surfactant complexes and micelles in $C_8\beta G_1$ solutions (35 mM) (*A*) and in $C_9\beta G_1$ solutions (15 mM) (*B*).

perhaps unsurprisingly, that the micelles are more flexible than the PDCs.

Modeling of BR-$C_8\beta G_1$ complexes by the sphere method

The complexes formed by BR and $C_8\beta G_1$ were approximated by an aggregate of sufficiently small spheres. The surfactant subunit was modeled as a featureless shell composed of spheres, each weighted by the calculated average scattering length density of $C_8\beta G_1$. In this calculation, the headgroup of the alkyl monoglucosides was assumed to be strongly hydrated, with four solvent molecules bound to each glucose (49). The length of the surfactant shell was set equal to 30 Å, which is the measured hydrophobic length of bacteriorhodopsin (45).

The pair distance distribution function of the modeled PDCs was computed for surfactant shells with fixed length and variable thickness. Increments of 3 Å were used for the shell thickness in these calculations. By comparing these functions with the experimental $p(r)$ determined in the IFT analysis, it is possible to estimate the thickness of the shell of surfactant around bacteriorhodopsin. The best agreement was obtained for a shell thickness of 15 ± 3 Å (Fig. 8).

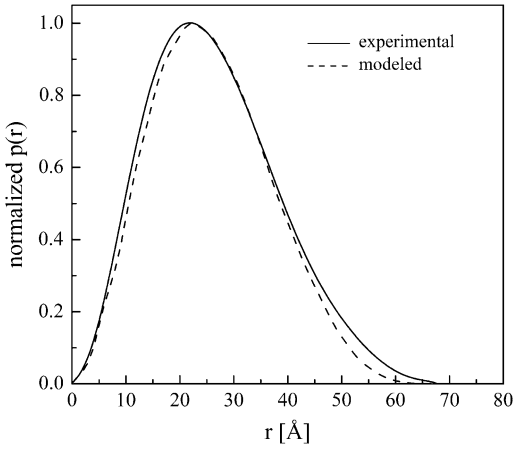

FIGURE 8 Comparison between the experimental (IFT) and the modeled (sphere method) $p(r)$ of BR-$C_8\beta G_1$ complexes. The thickness of the modeled surfactant shell is 15 Å.

DISCUSSION

Membrane proteins are often characterized by poor stability when solubilized in surfactant solutions. Understanding how surfactants self-assemble around these proteins and affect their stability is important for optimal manipulation of these proteins outside native membranes. The absorption optics of analytical ultracentrifuges has been used for the analysis of surfactant binding by membrane proteins in highly dilute samples, where interaction effects can be neglected and the structural properties of the sedimenting complex can be determined. In the sedimentation equilibrium experiments described here, BR concentrations of 6–10 μM (active monomer form) could be used, which correspond to volume fractions of at most 2×10^{-4}. Use of the retinal-bound form, the activity of which is characterized by absorption at 550 nm, allows measurements of concentration profiles in the visible region to be used to highlight the features of the sole active species. Contributions from nonspecific aggregates, which are generally retinal-free clusters and would contribute to the overall protein peak at 280 nm, can thereby be avoided. The result is a highly accurate measurement of only the protein monomers.

Surfactant binding by membrane proteins has been extensively studied by several approaches. Based on results from equilibration chromatography on various transmembrane proteins solubilized in solutions of Triton X-100, $C_{12}E_8$, and $C_{12}\beta G_2$, Moller and le Maire concluded that the general mode of binding by these proteins is consistent with a monolayer type of surfactant rather than a micellar one (50). BR represented an isolated case, as it was found to bind relatively high amounts of surfactant, so the PDCs were always significantly larger than the corresponding micelles. These results were explained in terms of the high hydro-

phobicity (~80% based on amino acid composition) and small size of BR, which could result in almost complete burial of the protein in the interior of the micelle. Furthermore, the binding did not change with the extent of delipidation of BR.

Analysis by sedimentation equilibrium clearly indicates that for BR the binding modality can vary from a single layer of surfactant to a larger shell. In general, the size of the surfactant shell is unrelated to the dimensions of the protein-free micelles, and can be larger or smaller than the corresponding micelles. When BR forms complexes with $C_8\beta G_1$, the amount of bound surfactant is comparable to the micellar aggregation number at 35 mM $C_8\beta G_1$, but it does not change at concentrations where larger micelles exist. In fact, BR binds approximately the same number of surfactant molecules of $C_8\beta G_1$ at 70 mM as at 35 mM, within the precision of the experimental method, whereas the micellar aggregation number increases by 37%. This result corroborates the hypothesis that membrane proteins do not need a preformed micelle to be solubilized. Future investigations with other surfactants will test the generality of this behavior. No direct correlation can be established between the amount of bound surfactant and its free monomer concentration. For example, the protein binds approximately the same number of surfactant monomers in solutions with $C_9\beta G_1$ as it does for $C_{12}\beta G_2$, two surfactants characterized by a 40-fold difference in their CMC values.

Results from the IFT analysis of membrane protein-surfactant solutions indicate that the PDC shape is significantly different from that of the corresponding micelles. In addition to the findings of surfactant binding from the contrast variation studies, this suggests that membrane proteins are not embedded in preformed micelles. Rather, surfactant molecules shield the hydrophobic region of the protein by forming a shell of a thickness that varies with the type of surfactant. This hypothesis was proposed by le Maire et al. (1), who suggested monolayer rings as the most probable structure of surfactant bound by membrane proteins. However, they also excluded any structure where the surfactant is not in direct contact with the protein (51).

The SANS studies of BR confirm that it binds significantly more of the longer-chain $C_9\beta G_1$ than of its homolog $C_8\beta G_1$. The amount of $C_9\beta G_1$ bound is not consistent with a monolayer arrangement around BR. Instead, increasing the length of the alkyl chain of the glucoside by one methylene group causes drastic changes in the micellar morphology. The ratio of the fitted micellar length to the diameter is 2.5 for $C_8\beta G_1$, whereas it is 15.1 for $C_9\beta G_1$. Nilsson et al. reported a similar value for the axial ratio of $C_8\beta G_1$ using NMR self-diffusion experiments in water (52), but an axial ratio of only 11 for $C_9\beta G_1$. However, they used a rigid prolate model for the $C_9\beta G_1$ micelles, whereas the SANS data here could be fitted best using the semiflexible model.

When the stability of BR is monitored over time by spectroscopy, the same trend of increase in stability with longer surfactant chains is observed for homologs of both the monoglucosides and the maltosides. The higher stability of bacteriorhodopsin in $C_9\beta G_1$ than in $C_8\beta G_1$ was previously recognized (53,54). Further, stability of solubilized rhodopsin was correlated with the length of the surfactant alkyl tail, and generally increased in solutions of longer chain amphiphiles (55). However, the properties of the surfactant headgroup also appear to have a critical role in promoting protein stability. Indeed, surfactants with the same tails but different headgroups have remarkably different effects on the stability of BR (Fig. 1).

The patterns of stability of the bacteriorhodopsin are rationalized in terms of the thickness of the surfactant layer at the hydrophobic interface of the protein, and how that thickness compares with the length of a single surfactant molecule. Because of the polarity of the molecule, shells made of a single layer of surfactants are highly curved and form an environment significantly different from the native lipid bilayer. On the other hand, when the membrane protein is embedded in larger shells of surfactants, the detergent molecules that are in contact with the hydrophobic surface of the protein, and further away from the curved end of the shell, are more likely to be oriented parallel to the transmembrane helices. In this case the interaction between the amphiphile alkyl chains and the protein helices is more similar to those within the lipid membrane. In fact, the helical turns of membrane proteins are highly interdigitated with the alkyl chains of the surrounding lipid molecules (56,57), and structure destabilization has been shown to occur when altering specific protein-lipid interactions by directed mutagenesis (58,59). Then, altering the surfactant tail packing around solubilized membrane proteins should affect the stability of the protein. In addition, larger surfactant shells are likely to exert a higher lateral pressure on the transmembrane helices than single surfactant layers, thereby favoring tertiary contacts between the helices that keep the chromophore in its functional conformation. Supporting this hypothesis is the observation that $C_8\beta G_1$-solubilized BR exhibits a much higher hydrogen/deuterium exchange of the peptide protons (65%) than in purple membrane (40%), indicating that the accessibility of the solvent to the protein interior has increased in the solubilized state (60). This situation was found to be linked to irreversible denaturation of the protein, which, in fact, occurs through destabilization of the helical assembly and consequent loss of the chromophore contacts.

There is substantial evidence that the surfactants optimal for membrane protein stability are not always the best for crystallization. Specifically, BR crystals have been grown in solutions of $C_8\beta G_1$, where the protein stability is limited to a few days, whereas attempts using its homolog $C_9\beta G_1$, in which BR is highly stable, have failed (61,62). Nucleation of the BR-$C_8\beta G_1$ complex is indeed favored from the single-layer arrangement of bound surfactant because protein-protein hydrophilic contacts are not sterically hindered as in solutions of $C_9\beta G_1$, where the hydrophobic domain of BR is

surrounded by a much larger surfactant shell. However, the limited stability of BR in $C_8\beta G_1$ (a few days) often resulted in poorly ordered crystals. Subsequently, the alternative approach of lipidic cubic phases was devised and produced BR crystals with high-resolution diffraction properties (63,64).

CONCLUSIONS

Contrast variation techniques in sedimentation equilibrium and small-angle neutron scattering studies have revealed the properties of surfactant binding by BR in solutions of alkyl monoglucosides and alkyl maltosides with chains containing from 8 to 12 carbons. These features are related to the stability patterns monitored by UV-visible spectroscopy, and the protein stability in a surfactant environment directly correlates with the thickness of the bound surfactant layer. Specifically, surfactants that bind to BR as single layers offer poor stability over time. Optimal levels of stability for BR are achieved in solutions of $C_9\beta G_1$ and $C_{12}\beta G_2$, where the numbers of bound surfactant molecules are comparable. In each individual class of surfactant (glucosides or maltosides), molecules with shorter alkyl chains generally bind as single layers, whereas longer-chain surfactants bind in shells of increasing thickness. No relation was found between the number of surfactant molecules bound to the protein and the aggregation number of the corresponding protein-free micelles. As a consequence, membrane proteins are solubilized in a highly cooperative process that depends on the properties of the surfactant molecule, rather than being incorporated in preformed micelles.

For complexes of BR and $C_8\beta G_1$, the surfactant arrangement around the hydrophobic region of the protein can be reconstructed by comparing the experimentally determined pair distance distribution functions with those computed using the sphere method approximation. The shell of $C_8\beta G_1$ bound to BR is made of a single layer of surfactant that is bound around the hydrophobic region of the protein. This geometry is consistent with the findings from the sedimentation equilibrium experiments.

These results are a useful heuristic guide toward the rational selection of surfactant solutions for optimal solubilization of membrane proteins. Such selection will increase success rates in crystallization and functional studies of these proteins.

We acknowledge the National Institute of Standards and Technology, U.S. Department of Commerce, for providing the neutron research facilities used in this work, which were supported in part by the National Science Foundation under Agreement No. DMR-0454672. We are thankful to G. Turner (Seton Hall University) for kindly providing the *Halobacterium salinarum* strain, B. Berger for assistance with the cell growth, and G. Fritz (University of Graz) for providing the program for the IFT analysis. The Delaware Biotechnology Institute and the Center of Biomedical Research Excellence (COBRE) in Membrane Protein Production and Characterization at the University of Delaware are acknowledged for use of their facilities.

COBRE is supported by the National Center for Research Resources of the National Institutes of Health (grant P20 RR015588). Funding for this work was from the Microgravity Research Program of NASA (grant NAG8-1830).

REFERENCES

1. le Maire, M., P. Champeil, and J. V. Moller. 2000. Interaction of membrane proteins and lipids with solubilizing detergents. *Biochim. Biophys. Acta.* 1508:86–111.
2. Tani, H., T. Saitoh, T. Kamidate, T. Kamataki, and H. Watanabe. 1997. Selective solubilization of microsomal electron-transfer proteins with alkylglucoside. *Anal. Sci.* 13:747–751.
3. Hunte, C., G. von Jagow, and H. Schagger. 2003. Membrane Protein Purification and Crystallization: A Practical Guide. Academic Press, New York.
4. Epand, R. M., E. H. Braswell, C. M. Yip, R. F. Epand, and S. Maekawa. 2003. Quaternary structure of the neuronal protein NAP-22 in aqueous solution. *Biochim. Biophys. Acta.* 1650:50–58.
5. Solovyova, A., P. Schuck, L. Costenaro, and C. Ebel. 2001. Non-ideality by sedimentation velocity of halophilic malate dehydrogenase in complex solvents. *Biophys. J.* 81:1868–1880.
6. Friesen, R. H. E., J. Knol, and B. Poolman. 2000. Quaternary structure of the lactose transport protein of *Streptococcus thermophilus* in the detergent-solubilized and membrane-reconstituted state. *J. Biol. Chem.* 275:33527–33535.
7. Tanford, C., and J. A. Reynolds. 1976. Characterization of membrane proteins in detergent solutions. *Biochim. Biophys. Acta.* 457:133–170.
8. Reynolds, J. A., and C. Tanford. 1976. Determination of molecular-weight of protein moiety in protein-detergent complexes without direct knowledge of detergent binding. *Proc. Natl. Acad. Sci. USA.* 73:4467–4470.
9. Kleinekofort, W., L. Germeroth, J. A. Vandenbroek, D. Schubert, and H. Michel. 1992. The light-harvesting complex-II (B800/850) from *Rhodospirillum molischianum* is an octamer. *Biochim. Biophys. Acta.* 1140:102–104.
10. O'Neill, H., W. T. Heller, K. E. Helton, V. S. Urban, and E. Greenbaum. 2007. Small-angle x-ray scattering study of photosystem I-detergent complexes: implications for membrane protein crystallization. *J. Phys. Chem. B.* 111:4211–4219.
11. Svergun, D. I. 2000. Advanced solution scattering data analysis methods and their applications. *J. Appl. Cryst.* 33:530–534.
12. Svergun, D. I., and M. H. J. Koch. 2003. Small-angle scattering studies of biological macromolecules in solution. *Rep. Prog. Phys.* 66:1735–1782.
13. Belrhali, H., P. Nollert, A. Royant, C. Menzel, J. P. Rosenbusch, E. M. Landau, and E. Pebay-Peyroula. 1999. Protein, lipid and water organization in bacteriorhodopsin crystals: a molecular view of the purple membrane at 1.9 Å resolution. *Structure.* 7:909–917.
14. Luecke, H., B. Schobert, H. T. Richter, J. P. Cartailler, and J. K. Lanyi. 1999. Structure of bacteriorhodopsin at 1.55 Å resolution. *J. Mol. Biol.* 291:899–911.
15. Oesterhelt, D., and W. Stoeckenius. 1971. Rhodopsin-like protein from purple membrane of *Halobacterium halobium*. *Nature.* 233:149.
16. Dencher, N. A., and M. P. Heyn. 1979. Bacteriorhodopsin monomers pump protons. *FEBS Lett.* 108:307–310.
17. Glasoe, P. K., and F. A. Long. 1960. Use of glass rlectrodes to measure acidities in deuterium oxide. *J. Phys. Chem.* 64:188–190.
18. Blandamer, M. J., P. M. Cullis, and J. Engberts. 1998. Titration microcalorimetry. *J. Chem. Soc., Faraday Trans.* 94:2261–2267.
19. Dencher, N. A., and M. P. Heyn. 1982. Preparation and properties of monomeric bacteriorhodopsin. *Methods Enzymol.* 88:5–10.
20. Rehorek, M., and M. P. Heyn. 1979. Binding of all-*trans*-retinal to the purple membrane: evidence for cooperativity and determination of the extinction coefficient. *Biochemistry.* 18:4977–4983.
21. Zhou, X., and G. Arthur. 1992. Improved procedures for the determination of lipid phosphorus by malachite green. *J. Lipid Res.* 33:1233–1236.

22. Wildenauer, D., and H. G. Khorana. 1977. Preparation of lipid-depleted bacteriorhodopsin. *Biochim. Biophys. Acta.* 466:315–324.

23. Buschmann, N., and S. Wodarczak. 1995. Analytical methods for alkylpolyglucosides. Part I: Colorimetric determination. *Tenside Surf. Det.* 32:336–339.

24. Yphantis, D. A. 1964. Equilibrium ultracentrifugation of dilute solutions. *Biochemistry.* 3:297–317.

25. Fujita, H. 1975. Foundations of Ultracentrifugal Analysis. Wiley & Sons, New York.

26. Reynolds, J. A., and D. R. McCaslin. 1985. Determination of protein molecular weight in complexes with detergent without knowledge of binding. *Methods Enzymol.* 117:41–53.

27. Edelstein, S., and H. Schachman. 1967. Simultaneous determination of partial specific volumes and molecular weights with microgram quantities. *J. Biol. Chem.* 242:306–311.

28. Renner, C., B. Kessler, and D. Oesterhelt. 2005. Lipid composition of integral purple membrane by H-1 and P-31 NMR. *J. Lipid Res.* 46:1755–1764.

29. Harpaz, Y., M. Gerstein, and C. Chothia. 1994. Volume changes on protein folding. *Structure.* 2:641–649.

30. Durchschlag, H., and R. Jaenicke. 1982. Partial specific volume changes of proteins: densimetric studies. *Biochem. Biophys. Res. Commun.* 108: 1074–1079.

31. Laue, T. M., B. D. Shah, T. M. Ridgeway, and S. L. Pelletier. 1992. Computer-aided interpretation of analytical sedimentation data for proteins. *In* Analytical Ultracentrifugation in Biochemistry and Polymer Science. S. E. Harding, A. J. Rowe, and J. C. Horton, editors. Royal Society of Chemistry, Cambridge, UK. 90–125.

32. Bacon, G. E. 1975. Neutron Diffraction. Clarendon Press, Oxford, UK.

33. Englander, S. W., N. W. Downer, and H. Teitelbaum. 1972. Hydrogen exchange. *Annu. Rev. Biochem.* 41:903–924.

34. Konishi, T., and L. Packer. 1977. Hydrogen exchange of dark-adapted and illuminated bacteriorhodopsin. *FEBS Lett.* 80:455–458.

35. Earnest, T. N., J. Herzfeld, and K. J. Rothschild. 1990. Polarized Fourier transform infrared spectroscopy of bacteriorhodopsin. Transmembrane α-helices are resistant to hydrogen/deuterium exchange. *Biophys. J.* 58:1539–1546.

36. Pedersen, J. S. 1997. Analysis of small-angle scattering data from colloids and polymer solutions: modeling and least-squares fitting. *Adv. Colloid Interface Sci.* 70:171–210.

37. Brunner-Popela, J., and O. Glatter. 1997. Small-angle scattering of interacting particles. 1. Basic principles of a global evaluation technique. *J. Appl. Cryst.* 30:431–442.

38. Glatter, O., G. Fritz, H. Lindner, J. Brunner-Popela, R. Mittelbach, R. Strey, and S. U. Egelhaaf. 2000. Nonionic micelles near the critical point: micellar growth and attractive interaction. *Langmuir.* 16:8692–8701.

39. Kotlarchyk, M., and S. H. Chen. 1983. Analysis of small-angle neutron scattering spectra from polydisperse interacting colloids. *J. Chem. Phys.* 79:2461–2469.

40. Glatter, O. 1980. Computation of distance distribution functions and scattering functions of models for small-angle scattering experiments. *Acta Phys. Austriaca.* 52:243–256.

41. Tanford, C., Y. Nozaki, J. A. Reynolds, and S. Makino. 1974. Molecular characterization of proteins in detergent solutions. *Biochemistry.* 13:2369–2376.

42. Reference deleted in proof.

43. Reference deleted in proof.

44. VanAken, T., S. Foxall-VanAken, S. Castleman, and S. Ferguson-Miller. 1986. Alkyl glycoside detergents: synthesis and applications to the study of membrane proteins. *Methods Enzymol.* 125:27–35.

45. Piknova, B., E. Perochon, and J. F. Tocanne. 1993. Hydrophobic mismatch and long-range protein-lipid interactions in bacteriorhodopsin phosphatidylcholine vesicles. *Eur. J. Biochem.* 218:385–396.

46. Tanford, C. 1980. The Hydrophobic Effect: Formation of Micelles and Biological Membranes. Wiley & Sons, New York.

47. Guinier, A., and G. Fournet. 1955. Small Angle Scattering of X-rays. Chapman and Hall, London.

48. Pedersen, J. S., and P. Schurtenberger. 1996. Scattering functions of semiflexible polymers with and without excluded volume effects. *Macromolecules.* 29:7602–7612.

49. He, L. Z., V. Garamus, B. Niemeyer, H. Helmholz, and R. Willumeit. 2000. Determination of micelle structure of octyl-β-glucoside in aqueous solution by small angle neutron scattering and geometric analysis. *J. Mol. Liq.* 89:239–248.

50. Moller, J. V., and M. le Maire. 1993. Detergent binding as a measure of hydrophobic surface area of integral membrane proteins. *J. Biol. Chem.* 268:18659–18672.

51. Le Maire, M., S. Kwee, J. P. Andersen, and J. V. Moller. 1983. Mode of interaction of polyoxyethyleneglycol detergents with membrane-proteins. *Eur. J. Biochem.* 129:525–532.

52. Nilsson, F., O. Söderman, P. Hansson, and I. Johansson. 1998. Physical-chemical properties of C_9G_1 and $C_{10}G_1$ β-alkylglucosides. Phase diagrams and aggregate size/structure. *Langmuir.* 14:4050–4058.

53. Miercke, L. J. W., P. E. Ross, R. M. Stroud, and E. A. Dratz. 1989. Purification of bacteriorhodopsin and characterization of mature and partially processed forms. *J. Biol. Chem.* 264:7531–7535.

54. Michel, H., and D. Oesterhelt. 1982. Preparation of new two-dimensional and 3-dimensional crystal forms of bacteriorhodopsin. *Methods Enzymol.* 88:111–117.

55. De Grip, W. J. 1982. Thermal stability of rhodopsin and opsin in some novel detergents. *Methods Enzymol.* 81:256–265.

56. Garavito, R. M., and S. Ferguson-Miller. 2001. Detergents as tools in membrane biochemistry. *J. Biol. Chem.* 276:32403–32406.

57. Capaldi, R. A., editor. 1977. Membrane Proteins and their Interactions with Lipids. Marcel Dekker, New York.

58. Fleming, K. G. 2000. Probing stability of helical transmembrane proteins. *Methods Enzymol.* 323:63–77.

59. Fyfe, P. K., N. W. Isaacs, R. J. Cogdell, and M. R. Jones. 2004. Disruption of a specific molecular interaction with a bound lipid affects the thermal stability of the purple bacterial reaction centre. *Biochim. Biophys. Acta.* 1608:11–22.

60. Sonoyama, M., T. Hasegawa, T. Nakano, and S. Mitaku. 2004. Isomerization of retinal chromophore and conformational changes in membrane protein bacteriorhodopsin by solubilization with a mild nonionic detergent, *n*-octyl-β-glucoside: an FT-Raman and FT-IR spectroscopic study. *Vib. Spectrosc.* 35:115–119.

61. Garavito, R. M., Z. Markovic-Housley, and J. A. Jenkins. 1986. The growth and characterization of membrane protein crystals. *J. Cryst. Growth.* 76:701–709.

62. Michel, H. 1982. Characterization and crystal packing of 3-dimensional bacteriorhodopsin crystals. *EMBO J.* 1:1267–1271.

63. Landau, E. M., and J. P. Rosenbusch. 1996. Lipidic cubic phases: a novel concept for the crystallization of membrane proteins. *Proc. Natl. Acad. Sci. USA.* 93:14532–14535.

64. Pebay-Peyroula, E., G. Rummel, J. P. Rosenbusch, and E. M. Landau. 1997. X-ray structure of bacteriorhodopsin at 2.5 Å from microcrystals grown in lipidic cubic phases. *Science.* 277:1676–1681.